SSRG International Journal of Electronics and Communication Engineering
ISSN: 2348-8549/ https://doi.org/10.14445/23488549/IJECE-V13I7P124

Volume 13 Issue 7, 335-346, July 2026

Original Article

Performance Evaluation of a Deep Learning-based Optimal Image Compression Scheme in Two Distinct Wireless Models

Shaiba Akhter[1], Rupaban Subadar[2], Sushanta Kabir Dutta[3]

[1,2,3]*Department of Electronics and Communication Engineering, North Eastern Hill University, Meghalaya, India.*

[1]*Corresponding Author : shaibaakhter123@gmail.com*

Received: 13 March 2026 Revised: 06 May 2026 Accepted: 06 June 2026 Published: 29 July 2026

Abstract *- The need for dependable transmission of high-quality images across wireless communication networks has grown due to the quick expansion of multimedia applications, including web services, digital photography, and medical imaging. Wireless channels, however, are particularly vulnerable to multipath fading, which raises the Bit Error Rate (BER), causes data loss, and deteriorates system performance. Therefore, reliable transmission techniques and efficient image compression are essential to ensure high-quality image delivery in poor channel circumstances. In this regard, this manuscript proposes an effective deep learning-based image compression framework intended to maintain image quality during wireless transmission as a solution to this problem. This manuscript first examines an autoencoder-based optimum compression strategy. The proposed autoencoder compression scheme obtains PSNR values of 24.81 dB and 27.58 dB, low MSE values of 0.004 and 0.002, and compression ratios of 0.38 and 0.75, respectively, according to performance evaluation using the Microsoft COCO and CIFAR-10 datasets. Secondly, using different modulation techniques like QPSK and BPSK with and without diversity schemes, the compressed images are transmitted over simple and sophisticated wireless channel models, like the Rayleigh fading and Nakagami-m fading channel models, respectively. According to experimental data, diversity-assisted modulation achieves PSNR values between 43.39 dB and 55.18 dB, greatly improving visual fidelity and transmission dependability. The proposed method successfully strikes a balance between the effectiveness of compression and image quality, making it a viable option for wireless multimedia communication in difficult channel circumstances.*

Keywords *- Image Compression, Deep Learning, Autoencoder, Diversity, Selection Combining*.

1. Introduction

Wireless Communication is one of the most prevalent and intriguing technologies that is increasingly permeating our daily lives. Advancement of wireless technology has significantly changed several industries, including smart infrastructure, telecommunications, healthcare, and transportation. Modern digital infrastructure is built on wireless communication, which enables fast data transfer, easy access to information, and worldwide connectivity. As societies become more reliant on mobile and wireless solutions, advances in wireless communication have become crucial for ensuring reliable, high-performance networks that enable a wide range of applications. Wireless devices are used by a large number of individuals worldwide for communication and information sharing [1].

These days, the most important sort of media that people carry with them throughout their lives is sharing pictures and videos. The fastest-growing applications in modern wireless communication systems require high-quality visual data, especially in challenging channel conditions. The exponential growth of multimedia data in today's data-driven culture presents significant challenges for data transfer, storage, and program efficiency because of the massive volumes of these files [2].

Due to the growing number of applications that require high-quality visual data even under difficult channel conditions, efficient image transmission has become more and more important in contemporary wireless communication systems. For applications like augmented reality, remote sensing, autonomous driving, and the Internet of Things (IoT), timely and dependable image transmission is essential [3, 4].

As multimedia information continues to grow exponentially in today's data-driven culture, the massive amount of these files presents significant issues for data transmission, storage, and overall system performance. To overcome these difficulties, data compression methods have been created with the goal of minimizing the size of multimedia files without sacrificing their quality. Among these, image data compression is essential for lowering the amount of bandwidth and storage space needed for images [5].

Consequently, image compression has emerged as a practical solution to these issues, prompting extensive research into developing efficient compression techniques. Images are employed in a variety of industries, including topography mapping and medical imaging. For efficient transmission, the images must be compressed and represented in a reduced format [6]. As data volumes rise, especially in multimedia applications, effective compression techniques become more crucial. These compression techniques aim to remove unnecessary information without detracting from the perceived quality of the original data. Eliminating extraneous information from the material being compressed is the secret to many compression techniques.

Image Compression algorithms aim to minimise data size without significantly compromising image quality. The goal of image compression techniques is to maximise storage capacity while enabling faster transmission. The method of shrinking an image file while preserving its fundamental properties is known as image compression. Images may be stored and transmitted over constrained bandwidth channels more easily due to this size decrease. The compression ratio and image quality are frequently used to gauge how well an image compression technique works. It has been the focus of years of research, and many image compression standards have been developed for various applications [7].

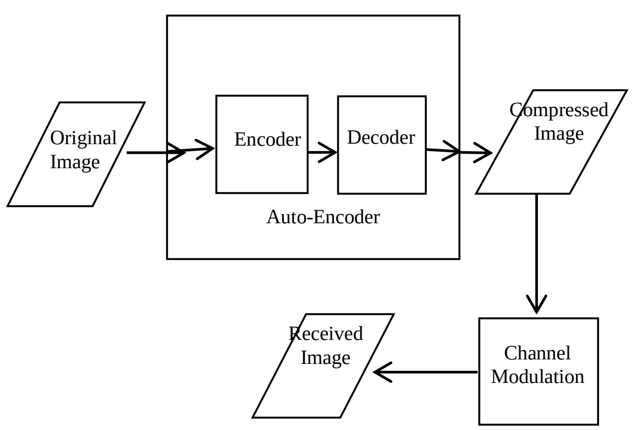

Fig. 1 A basic block diagram representing our work

2. Image Compression Standards

Understanding the fundamentals of image compression is crucial for grasping newer methods. Over the years, many common traditional image compression schemes, including JPEG, JPEG2000, PNG, etc, have evolved over time. The image compression techniques that were created to preserve a balance between file size and image quality are based on these standards.

2.1. Traditional Image Compression Approaches

2.1.1. JPEG

To develop a useful image compression standard, the Joint Photographic Experts Group (JPEG) was initially founded in 1987. The JPEG compression method is considered the foundation or standard algorithm that remains in use today and has established the standard for all subsequent compression methods. JPEG became an international standard in 1992. Uploading and sharing digital photographs online, which work with almost all image processors and browsers, is one of its most popular uses.

The most popular lossy compression method is JPEG, which breaks down an image into its component frequencies using the Discrete Cosine Transform (DCT). JPEG attains large compression ratios with comparatively little perceptual quality loss by quantising less significant frequencies. In the imaging and multimedia sectors, it is commonly used [8, 9].

2.1.2. JPEG2000

Based on wavelet transforms, JPEG2000 is an advancement over JPEG. Higher compression efficiency and improved quality are made possible by this, particularly for high-frequency images like medical imaging. Compared to the original JPEG, the JPEG-2000 image compression technique has a rate-distortion benefit. More significantly, it enables the extraction of various resolutions, pixel fidelities, components, regions of interest, and more from a single compressed bitstream. This enables a program to modify or send only the necessary data from any JPEG 2000 compressed source picture to any target device [10, 11].

2.1.3. PNG

Portable Network Graphics is a popular lossless picture format that makes use of several methods, including deflate compression. The method works by finding and removing redundant information in pixel data, especially in pictures that have a lot of consistent colour. As a result, the file size is significantly reduced without sacrificing image quality.

Web graphics, screenshots, and photos with transparency are examples of images with huge sections of solid colour or gradients that PNG is excellent at reducing. Unlike for the purpose of compression, PNG and JPEG do not sacrifice quality. Diagrams, logos, and typography are examples of crisp, clear graphics that perform incredibly well with it. PNG uses a variety of compression techniques, such as deflate compression and filtering algorithms [12].

2.2. Deep Learning-based Optimal Image Compression Approach

Artificial Intelligence in image compression has enabled innovative methods that can dynamically adapt to the content of images, yielding impressive compression ratios without compromising high visual quality. AI-based methods, particularly those utilising neural networks, have shown tremendous promise by facilitating more efficient encoding and decoding. With the most recent advances in deep learning, neural network-based methods have shown promising results in picture reduction. The use of picture compression has drastically changed with recent advances in Deep Learning (DL).

Deep Learning has advanced significantly in the field of picture compression in recent years, producing advantageous compression outcomes while preserving and achieving a desirable and appealing level of image quality. Both industry and academic research are interested in deep learning-based image compression, resulting in the creation of several compression methods with varying degrees of efficacy and success. To learn an efficient image representation that minimises file size without compromising quality, methods such as autoencoders are employed [13, 14].

2.2.1. Autoencoder-based Image Compression

An autoencoder is a type of neural network that can both encode and decode input; it is commonly used for noise reduction and dimensionality reduction. There are two primary components to it: By recognizing and keeping just the most crucial features while removing noise and extraneous information, an encoder compresses the input data. Encoder lowers image size step-by-step using convolution layers. Encoder transforms the image into a low-dimensional latent code, which is the latent space or the bottleneck layer that keeps the important information of the image and determines the compression ratio. The decoder then reconstructs the image from the latent code, striving to recover maximum visual quality. The main advantages of autoencoders are their ease of implementation and configuration, as well as their capacity to adapt to different data formats [15].

3. Literature Review

Throughout the years, the domain of image compression has seen tremendous growth, with several methods developed to address the challenges of efficient storage and transmission without sacrificing image quality. based on an examination of recent studies and publications. Conventional image compression techniques, such as PNG, JPEG, and JPEG2000, each have advantages and disadvantages. For instance, PNG maintains excellent image quality but produces bigger file sizes, whereas JPEG is good for photos but can introduce obvious artefacts when compressed too much [15].

A compressive autoencoder for image compression that combines CNNs with effective quantization and entropy encoding was proposed by Theis et al. [16]. Their technique surpassed JPEG and JPEG2000 in PSNR, SSIM, and Subjective Quality (MOS), especially at higher data rates. The compressed images had average bit rates of 0.244, 0.364, and 0.485. A scalable image compression technique utilizing an end-to-end autoencoder that predicts and reuses latent features was presented by MEI et al. [17].

Low-resolution images are produced by a base layer, while quality and resolution are increased by enhancement layers. The technique demonstrates superior rate-distortion performance on standard datasets, outperforming Single-Layer Techniques and Conventional Scaling Standards (SVC, SHVC) in bit-rate efficiency and image quality. A deep convolutional autoencoder that reduces bit rate in comparison to JPEG was presented by Cheng et al. [18] for image compression. By incorporating PCA to build energy-compact feature representations, the approach increases entropy coding and reconstructed image quality. On the Kodak dataset, it achieves approximately. 14% BD-rate reduction over JPEG2000, outperforming conventional image compression techniques.

Additionally, Aiswarya M et al. [19] concentrated on lossless and lossy compression algorithms, such as JPEG, JPEG2000, PNG, and more recent deep learning-based techniques, where Autoencoder and other deep learning-based techniques significantly improve quality without sacrificing Compression Ratio (CR), Peak Signal-to-Noise Ratio (PSNR), or Structural Similarity Index (SSIM). They concluded that the emergence of deep learning-based methods presents exciting new directions for further study, particularly in achieving higher compression ratios without appreciably reducing perceptual quality.

Therefore, the capacity to deal with high-quality images and the retention of high texture and detail quality at low bit-rates are the main advantages of compression via deep learning. In summary, deep learning-based methods like Autoencoders enable the achievement of effective image compression, improving the balance between file size and visual quality. Considering the strengths and limitations of the above discussions, the autoencoder image compression scheme is selected for additional testing because of its operational characteristics and ease of use.

3.1. Research Gap and Subsequent Contribution

Existing research and literature indicate that the performance of Autoencoder-based image compression has not previously been examined in the context of wireless fading channels**.** In this manuscript, a thorough analysis has been carried out for both the Rayleigh fading channel and the Nakagami-m fading channel, and manuscript contributions are listed below:

- Sections 2 and 3 provide an empirical overview of conventional image compression techniques, their drawbacks, and current developments based on deep learning.
- Second, to increase the use of image compression in wireless communication, sections 4 and 5 provide a brief description of the theory behind the Deep Learning-based optimal image compression scheme, or Autoencoder,

outlining its theoretical underpinnings and assessing its performance by calculating its CR, PSNR, and MSE.

- Thirdly, the use of diversity in Wireless Channel models-the Rayleigh model and the Nakagami-m fading model-using various modulation schemes like QPSK and BPSK is briefly described in section 6.
- Lastly, the methodology is described in Section 7, along with the integration of the Rayleigh model and the Nakagami-m fading model with the chosen optimal image compression technique. Using performance curves, bar charts, and comparative tables, Section 8 shows the evaluation and simulation findings and determines the optimal modulation approach.

4. Key Metrics for Assessing the Optimal Compression Method

The effectiveness and performance of these two compression algorithms have been assessed using three performance evaluation criteria. They are as follows:

4.1. Peak Signal-to-Noise Ratio (PSNR)

The ratio between the maximum image power and the noise corruption power that degrades the representation quality is known as the peak signal-to-noise ratio. For example, measuring the peak error between the compressed and original images. A higher PSNR indicates higher image quality [20].

$$PSNR = 10\, log_{10} \frac{R_I^2}{MSE} \quad (1)$$

Where R_I is the maximum possible pixel value of the image.

4.2. Mean Square Error (MSE)

It shows the total squared error between the original and compressed images. A tiny bit of MSE improves image quality and lowers mistakes. A small amount of MSE reduces errors and enhances the quality of images [21].

$$MSE = \frac{\sum_{i=1}^{M}\sum_{j=1}^{N}[I(i,j)-K(i,j)]^2}{M \times N} \quad (2)$$

Where $I(i,j)$ is the pixel value of the original image, and $K(i,j)$ is the pixel value of the compressed image. And $M \times N$ are the dimensions of the images.

4.3. Compression Ratio

Defined as the ratio of the data of the actual image to that of the data of the compressed image [22]

$$CR = \frac{N_1}{N_2} \quad (3)$$

Where N_1 is the original image size and N_2 is the compressed image size.

5. Proposed Model for Image Compression

5.1. Model Architecture

5.1.1. Encoder

The input images are compressed into smaller representations by the encoder, which consists of three convolutional blocks. Each of the three convolutional blocks has a CONV2D layer with ReLU activation, "Same" padding, Batch Normalisation to speed up and stabilise training, MaxPooling2D for down-sampling, and Dropout to avoid overfitting. To provide non-linearity, the three convolutional blocks apply 64, 128, and 256 convolutional filters with ReLU activation to each 3x3 input picture. "Same" padding guarantees that the output's dimensions match those of the input. The convolutional layer's output is guaranteed by the batch normalisation layer, which enhances training performance and stability. The MaxPooling2D layer efficiently performs down-sampling by reducing the input's spatial dimension. During training, the dropout layer randomly sets a fraction of the input units to 0 to prevent overfitting.

5.1.2. Latent Space

This is a lower-dimensional feature space that represents the compressed representation of the input images.

5.1.3. Decoder

The compressed representation is rebuilt to the original image size by the Model Architecture's decoder component. To expand the spatial dimensions, it employs several convolutional and upsampling layers. The Deconvolutional block applies 256, 128, and 64 convolutional filters with ReLU activation to each 3x3 input. Once more, the output of the convolutional layer is normalised using the Batch Normalization layer. The spatial dimensions are increased by the upsampling 2D layer. In order to create the final reconstructed image with normalised pixel values, the output layer's CONV2D layer applies three convolutional filters to the input using Sigmoid activation.

5.2. Dataset Description

A popular large-scale dataset for computer vision tasks like object detection, segmentation, key point detection, and picture captioning is the Microsoft Common Objects in Context (COCO) dataset. It is a benchmark dataset intended to promote study on a variety of object types and intricate sceneries. It contains 5000 images of size 512×512. These datasets are mainly used to assess the models' correctness and obtain an objective performance assessment. The COCO dataset is intended to depict a wide range of objects that we frequently come across in daily life, including people, cars, and animals like dogs. The COCO dataset is used as a benchmark model more successfully than small-scale datasets because it includes images from over 80 "object" and 91 generic "stuff" categories. Convolutional Neural Networks (CNNs) are frequently evaluated using CIFAR-10 due to their tiny image size and complexity. The CIFAR-10 dataset contains six thousand (6000) images of size 32 × 32. It has become the benchmark for evaluating new models and algorithms and is widely used for tasks including feature extraction, object recognition, and image classification [23, 24].

This work makes use of the Microsoft COCO and CIFAR-10 datasets, even though several high-resolution picture datasets, like the DIV2K and Kodak Dataset, are frequently utilised for assessing image compression algorithms. The main justification is that these datasets offer a vast array of varied images with various objects, textures, and scene variations, which are helpful for training and assessing deep learning models like autoencoders. Additionally, COCO gives more complicated real-world visual information for assessing reconstruction quality, whereas CIFAR-10 delivers low-resolution images appropriate for quick training and computing efficiency. These datasets are appropriate for assessing the suggested compression framework in wireless transmission scenarios because they facilitate efficient testing, lower computing costs, and enable the model to generalise well across various image types.

5.3. Comprehensive Comparison between Two Datasets

Using the CIFAR-10 and Microsoft COCO datasets, the Autoencoder image compression scheme's findings are shown in Table 1 below according to its Performance Evaluation Parameters, which include PSNR, MSE, and Compression Ratio (CR).

Table 1. Compression Results of the Autoencoder image compression framework

Key Metrics	Results for the Autoencoder image compression framework using different datasets	
	Microsoft COCO Dataset	CIFAR-10 Dataset
PSNR	24.81 dB	27.58 dB
MSE	0.004	0.002
CR	0.38	0.75

From the above analysis and results, we can conclude that autoencoders represent a well-balanced method of lowering image dimensions without sacrificing high image quality and are generally efficient for compression and need less computational complexity and expense since they produce reasonably strong PSNR ratios, low MSE, and a good compression ratio. Thus, an autoencoder image compression approach based on deep learning will be used on wireless models. Image transmission across wireless channels is even more challenging than in wired contexts because wireless communications systems are prone to fading phenomena that cause burst channel failures.

The main objective of image compression in wireless communication is to reduce image data size to enable more effective transmission via wireless networks or channels. Due to wireless communication's limited bandwidth, as well as faster transmission, lower power consumption, and increased storage efficiency, etc., there is a growing need for an effective compression method.

For instance, uploading an uncompressed image would either take a long time or drastically degrade image quality; occasionally, it might not even be uploaded. Therefore, when delivering an image over a wireless channel, it is better to employ an image compression method that is resistant to channel failures. Fading is a crucial component of channel estimation in wireless communication.

The sudden shift in the intensity of the received signal is known as fading. Communication systems are vulnerable to multipath fading caused by reflections from surrounding objects, refractions, and dispersion from buildings and other large structures. Decoded visual information may deteriorate significantly when images are delivered over noisy channels. A suitable system needs to be created in order to transmit images via a wireless channel. Diversification strategies have been developed to overcome this problem.

6. Use of Diversity in Wireless Channel Models

Diversity is a powerful communication technique that reduces the probability of deep fades by providing more than one copy of the transmitted signal to the receiver through different fading paths. Since fading is a random process, the possibility of a simultaneous deep fade at all the copies reduces considerably [25]. Space diversity is a relatively inexpensive and efficient communication technique that can be easily implemented with multiple antennas by keeping them a few wavelengths apart from each other.

Diversity improves coverage, data speeds, and the Signal-to-Noise Ratio (SNR) while lowering the Bit Error Rate (BER) [26]. In order to improve wireless communication reliability, this study employs the Selection Combining (SC) diversity technique in conjunction with a few modulation schemes. The SC method selects the best signals from the available diversity paths at the receiver. By estimating the current SNR value across all branches, the SC receiver chooses the branch with the best SNR for decoding [27, 28].

6.1. Wireless Channel Models

Various statistical models are being used to describe the fading in various physical environments. In this work, we have considered two widely used fading models for the transmission of our images. First, we consider the Rayleigh model and derive the expressions of BER and PSNR considering the SC diversity receiver. In the second work, we considered a Nakagami-m model, which is a complex model compared to the Rayleigh model, and derived the expressions for BER and PSNR.

6.1.1. Rayleigh Fading Model

The Rayleigh fading channel model has served as the foundation for the majority of theoretical studies on multiple antenna systems under scattering circumstances, and it continues to do so. The Rayleigh fading model is primarily used for a wireless environment when there is no line-of-sight path between the transmitter and receiver. Although this model is a preliminary channel model, researchers have been using it for a long time, and it has a lot of importance in the field of research. The Rayleigh fading channel amplitude's Probability Density Function (PDF) can be expressed as [30-32]:

$$P_\alpha(\alpha) = \frac{2\alpha}{\Omega} exp\left(-\frac{\alpha^2}{\Omega}\right), \qquad \alpha \geq 0 \tag{4}$$

Where $\Omega = E[\alpha^2]$ and $E[\cdot]$ is the expectation operator. A Rayleigh RV α can be modelled as $\alpha = |Z| = |X + jY|$, where X and Y are independent Gaussian RVs with zero mean and equal variances.

Mathematical Analysis of the Rayleigh Model

The following formula can be used to do the random variable transformation and obtain the SNR PDF of the Rayleigh fading channel from (4).

$$\gamma = \frac{E_b}{N_0}\alpha^2 \tag{5}$$

Where E_b is the energy per bit, and N_0 is the power spectral density of Gaussian noise. The ultimate outcome can be found in [30] as

$$f_\gamma(\gamma) = \frac{1}{\bar{\gamma}} exp\left(-\frac{\gamma}{\bar{\gamma}}\right) \tag{6}$$

By calculating the derivative of the product CDF of all the input branches, the SC receiver's output SNR PDF may be obtained. By carrying out the integration, which is provided below [30], the CDF of a single branch can be determined from (6).

$$\begin{aligned} Pr[\gamma \leq \gamma_{th}] &= \int_0^{\gamma_{th}} \frac{1}{\bar{\gamma}} exp\left(-\frac{\gamma}{\bar{\gamma}}\right) d\gamma \\ &= 1 - exp\left(-\frac{\gamma_{th}}{\bar{\gamma}}\right) \end{aligned} \tag{7}$$

From (7), the CDF expression of the L-SC receiver can be obtained as

$$F_{\gamma_{sc}}(\gamma_{sc}) = \left[1 - exp\left(-\frac{\gamma_{sc}}{\bar{\gamma}}\right)\right]^L \tag{8}$$

The output SNR PDF of the SC receiver was derived as [30] by using the derivative of (8).

$$\begin{aligned} f_{\gamma_{sc}}(\gamma_{sc}) &= \frac{L}{\bar{\gamma}}\left[1 - exp\left(-\frac{\gamma_{sc}}{\bar{\gamma}}\right)\right]^{L-1} \\ &\times exp\left(-\frac{\gamma_{sc}}{\bar{\gamma}}\right) \end{aligned} \tag{9}$$

By taking the statistical average of the conditional probability error $p_e(\in|\gamma)$ over the given PDF in (9), the BER expression for different modulation schemes can be given as

$$p_e = \int_0^\infty \quad p_e(\in|\gamma_{sc}) f_{\gamma_{sc}}(\gamma_{sc}) d\gamma_{sc} \tag{10}$$

For the binary coherent modulation$p_e(\in|\gamma_{sc}) = Q\left(\sqrt{2a\gamma_{sc}}\right)$, where $a = 0.5$ binary FSK and $a = 1$ BPSK. Now, putting the values in (10), we obtained

$$\begin{aligned} p_e = \int_0^\infty Q\left(\sqrt{2a\gamma_{sc}}\right) \frac{L}{\bar{\gamma}}\left[1 - exp\left(-\frac{\gamma_{sc}}{\bar{\gamma}}\right)\right]^{L-1} \\ \times exp\left(-\frac{\gamma_{sc}}{\bar{\gamma}}\right) d\gamma_{sc} \end{aligned} \tag{11}$$

The binomial theorem and the equations (A-8a and A-6) are used to solve the aforementioned integral of [31] as

$$\begin{aligned} p_e = \frac{L\Gamma(1.5)}{2}\sqrt{\frac{a\bar{\gamma}}{\pi}} \sum_{k=0}^{L-1} \binom{L-1}{k} \\ \times (-1)^k \frac{{}_2F_1\left(1, 1.5, 2, \frac{k+1}{k+1+a\bar{\gamma}}\right)}{(k+1+a\bar{\gamma})^{1.5}} \end{aligned} \tag{12}$$

Similarly, the SC receiver's BER can be assessed for different modulation schemes.

The following formula is used to calculate an image's peak SNR below

$$PSNR = 10\, log_{10}\left(\frac{255^2}{MSE}\right)(dB) \tag{13}$$

Where, $MSE = \frac{1}{M\times N}\sum_{i=1}^{M}\sum_{j=1}^{N}[f'(i,j) - f(i,j)]^2$, $M \times N$is the size of the image matrix,$f'(i,j)$ is the received image, and $f(i,j)$ is the transmitted image.

6.1.2. Nakagami-m Fading Model

The Nakagami-m distribution is appropriate for summarizing statistics of mobile radio transmission in complicated environments, such as metropolitan areas. It is widely accepted by the research community and design engineers due to its close agreement with theoretical and practical data. It also imitates a wide range of real-world fading scenarios with a single adjustable parameter.

This distribution is typically the best fit for indoor and terrestrial mobile multipath propagation, as well as ionospheric radio link scintillation. It has two parameters: a shape parameter $\boldsymbol{m}$ and a second parameter controlling the spread $\boldsymbol{\Omega}$. Additionally, the urban environment is frequently modelled using the Nakagami-m distribution, and the PDF [33, 34] of the envelope is given by:

$$p_\alpha(\alpha) = \frac{2m^m\alpha^{2m-1}}{\Omega^m\Gamma(m)} exp\left(-\frac{m\alpha^2}{\Omega}\right), \quad \alpha \geq 0 \tag{14}$$

Where the fading severity is determined by the parameter $m \geq 0.5$. The Nakagami-m distribution's PDF turns into the one-sided Gaussian distribution for m= 0.5.

Mathematical Analysis of the Nakagami-m Fading Model

Using the relation given in Equation (5), the SNR PDF of the Nakagami-m channel can be given as [33]

$$p_\gamma(\gamma) = \frac{m^m \gamma^{m-1}}{\bar{\gamma}^m \Gamma(m)} exp\left(-\frac{m\gamma}{\bar{\gamma}}\right), \tag{15}$$

From (15), the CDF expression can be obtained as,

$$F_\gamma(\gamma) = \frac{g\left(m, \frac{m\gamma}{\bar{\gamma}}\right)}{\Gamma(m)}, \tag{16}$$

Where $g(a, x) = \int_0^x t^{a-1} e^{-t} dt$is the lower incomplete gamma function. From (16), the CDF of the SC receiver over Nakagami-m fading can be given as:

$$F_{\gamma_{sc}}(\gamma_{sc}) = \left\{\frac{g\left(m, \frac{m\gamma_{sc}}{\bar{\gamma}}\right)}{\Gamma(m)}\right\}^L. \tag{17}$$

By differentiating (17), the PDF of the SC receiver can be obtained as given below.

$$f_{\gamma_{sc}}(\gamma_{sc}) = \frac{L}{\Gamma^L(m)}\left(\frac{m}{\bar{\gamma}}\right)^m {\gamma_{sc}}^{m-1} exp\left(-\frac{m\gamma_{sc}}{\bar{\gamma}}\right) \times \left\{g\left(m, \frac{m\gamma_{sc}}{\bar{\gamma}}\right)\right\}^{L-1}. \tag{18}$$

The Equation (10) can be used for deriving the BER expression as,

$$P_e = \frac{L}{\Gamma^L(m)}\left(\frac{m}{\bar{\gamma}}\right)^m \int_0^\infty Q\left(\sqrt{2a\gamma_{\mathrm{SC}}}\right){\gamma_{sc}}^{m-1} \times exp\left(-\frac{m\gamma_{sc}}{\bar{\gamma}}\right)\left\{g\left(m, \frac{m\gamma_{sc}}{\bar{\gamma}}\right)\right\}^{L-1} d\gamma_{\mathrm{SC}} \tag{19}$$

By using the formula [35, 8.352.1] and binomial theorem, after some algebraic arrangement, the BER expression can be given as

$$P_e = \frac{L}{\Gamma(m)}\left(\frac{m}{\bar{\gamma}}\right)^m \sum_{n=0}^{L-1}\binom{L-1}{n}(-1)^n \sum_{k_1=0}^{m-1}\sum_{k_2=0}^{m-1}\cdots\sum_{k_n=0}^{m-1} \frac{(m)^{\sum_{i=1}^n k_i}}{\prod_{i=1}^n\{\bar{\gamma} k_i!\}} \int_0^\infty Q\left(\sqrt{2a\gamma_{sc}}\right)\gamma_{sc}^{m+\sum_{i=1}^n k_i - 1} exp\left(-\frac{m(n+1)\gamma_{sc}}{\bar{\gamma}}\right) d\gamma_{sc} \tag{20}$$

By writing the Gaussian Q function in terms of the upper incomplete Gamma function as per [31, A 8a], after utilising [35, 6.455.1] to solve the integral, the final BER expression can be expressed as,

$$P_e = \frac{L}{\Gamma(m)}\left(\frac{m}{\bar{\gamma}}\right)^m \sum_{n=0}^{L-1}\binom{L-1}{n}(-1)^n \times \sum_{k_1=0}^{m-1}\sum_{k_2=0}^{m-1}\cdots\sum_{k_n=0}^{m-1} \frac{m^{\sum_{i=1}^n k_i}}{\prod_{i=1}^n(\bar{\gamma}^{k_i} k_i!)} \times \frac{\Gamma\left(m+\sum_{i=1}^n k_i\right)}{2}\left(\frac{\bar{\gamma}}{m(n+1)}\right)^{m+\sum_{i=1}^n k_i} \times {}_2F_1\left(m+\sum_{i=1}^n k_i, \frac{1}{2}; 1; -\frac{a\bar{\gamma}}{m(n+1)}\right) \tag{21}$$

7. Performance Analysis

To simulate realistic wireless communication settings with fast signal attenuation and multipath propagation, the selected optimal image compression scheme is integrated or combined with a simple and sophisticated wireless channel model, i.e., the Rayleigh Channel Model and the Nakagami-m fading model, both with and without diversity, using different modulation schemes: BPSK and QPSK.

7.1. BPSK and QPSK

Binary Phase Shift Keying (BPSK), a type of digital modulation technology, makes use of two distinct phase shifts to encode binary data. Due to its resilience to noise, it is one of the most straightforward types of phase modulation and is frequently utilised in communication systems. Because it calls for two phase shifts, it is also relatively simple to implement. Phases are altered in response to input bits 1 and 0 in this fundamental digital modulation process. Conversely, the modulation method known as Quadrature Phase Shift Keying (QPSK) makes use of four different carrier signal phase shifts to encode two bits of data into a single symbol. It is a PSK variant that combines two bits (00,01,10,11). There are four possible carrier phase shifts (0, 90, 180, and 270) that correspond to each of these bit combinations [36, 37].

8. Results and Discussion

8.1. Experimental Setup

The effectiveness of the suggested adaptive and progressive image compression system is assessed experimentally in both the Nakagami-m Fading Model and the Rayleigh Fading Model channel conditions. Three modulation configurations-Binary Phase Shift Keying (BPSK) without diversity, BPSK with two-branch Selection Combining, and Quadrature Phase Shift Keying (QPSK) with two-branch selection combining-are used in simulations to gradually increase the Signal-to-Noise Ratio (SNR) and investigate the impact of channel quality on the reconstructed image performance.

There are fewer signal distortions and a lower Mean Squared Error (MSE) between the original and reconstructed images when the SNR rises, and the noise power falls. Peak Signal-to-Noise Ratio (PSNR) increases when MSE decreases since PSNR and MSE are inversely correlated.

Higher PSNR values suggest better visual quality and reconstruction fidelity, making it one of the most popular objective measures for assessing the quality of reconstructed images. The following simulation results show how compressed image transmission performs under various modulation techniques, both with and without diversity, across different SNR levels. To demonstrate the efficacy of the suggested method, two representative image examples are given for both the Rayleigh and Nakagami-m fading channel models.

8.1.1. Results of Original and Compressed Images using the Autoencoder

The output of the original photos and their compressed images are displayed below in Figures 2 and 3.

Fig. 2 Outcome of the bus's original and compressed images

Fig. 3 Outcome of the people's original and compressed images

8.2. Results for the Rayleigh Model

8.2.1. Simulation Curves showing the Results of Peak SNR vs Average SNR for the Rayleigh Model using Three Different Modulation Techniques

The following simulation curves illustrate the variation of PSNR with Average SNR over the Rayleigh fading channel using three modulation schemes: BPSK without diversity, BPSK with 2-branch SC, and QPSK with 2-branch SC, evaluated on the Bus and People images. As the Average SNR per branch increases from 0 to 20 dB, all three schemes exhibit a steady improvement in PSNR, indicating enhanced image reconstruction quality as channel SNR increases. For e.g., in the simulation curve of the 'Bus' image, at 0 dB average SNR, the PSNR values are approximately 10.84 dB for 2-SC BPSK, while both no-diversity BPSK and 2-SC QPSK achieve around 8.3 dB, providing an initial diversity gain of nearly 2 dB for the 2-SC BPSK scheme.

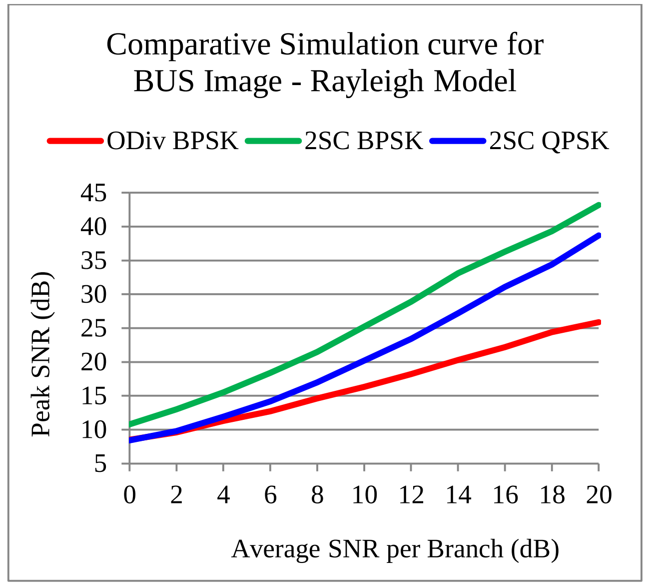

Fig. 4 Simulation results for the bus image

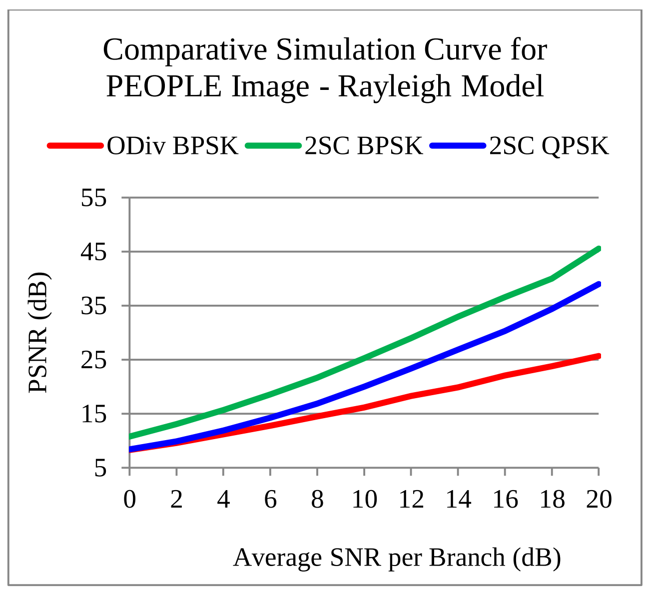

Fig. 5 Simulation result for the people image

At 10 dB, the PSNR increases to approximately 25.33 dB for 2-SC BPSK, compared with 20.27 dB for 2-SC QPSK and 16.31 dB for no diversity BPSK, representing improvements over the no diversity system. The performance gap becomes more significant at higher SNR values.

At 20 dB average SNR, 2-SC BPSK achieves the highest PSNR of approximately 43.39 dB, followed by 2-SC QPSK at 38.74 dB, whereas no diversity BPSK reaches only 25.90 dB.

Similarly, in the simulation curve of the ‘People’ image at 0 dB average SNR, the 2-SC BPSK scheme achieves the highest PSNR of approximately 10.87 dB, followed by no-diversity BPSK at 8.33 dB and 2-SC QPSK at 8.32 dB, indicating an initial diversity gain of nearly 2–3 dB. At 10 dB average SNR, the PSNR values increase to approximately 25.29 dB for 2-SC BPSK, 20.13 dB for 2-SC QPSK, and 16.29 dB for no-diversity BPSK, representing improvements over the non-diversity system.

The superiority of diversity reception becomes more evident at higher SNR values. At 20 dB Average SNR, 2-SC BPSK attains the highest PSNR of approximately 45.73 dB, while 2-SC QPSK reaches about 39.13 dB and no diversity BPSK achieves only 25.73 dB.

The results clearly show that BPSK with 2-branch SC consistently outperforms the other schemes for both images, achieving PSNR values in the range of 43.39–45.73 dB for the bus and people images, respectively. This superior performance demonstrates the effectiveness of diversity in mitigating fading effects, resulting in excellent image reconstruction quality and more reliable wireless image transmission.

For better comparative analysis, the results are also presented in tabular form for ‘Bus’ and ‘People’ images in Tables 2 and 3, respectively.

Table 2. Comparative quality analysis table showing the results of the bus image

SNR (in dB)	PSNR (in dB) for modulation techniques		
	BPSK (0 DIV)	BPSK (2 SC)	QPSK (2 SC)
0	8.3631	10.8475	8.332
2	9.6334	13.0604	9.9307
4	11.1625	15.5784	11.8945
6	12.7195	18.5482	14.2931
8	14.5066	21.7253	17.0062
10	16.3193	25.3318	20.2796
12	18.2371	28.8579	23.3432
14	20.2199	33.2512	27.1697
16	22.0795	36.4039	31.1751
18	24.1681	39.4142	34.5475
20	25.9052	43.3936	38.7447

Table 3. Comparative quality analysis table showing the results of the people image

SNR (in dB)	PSNR (in dB) for modulation techniques		
	BPSK (0 DIV)	BPSK (2 SC)	QPSK (2 SC)
0	8.3359	10.874	8.3277
2	9.656	13.0802	9.9271
4	11.1658	15.6199	11.8306
6	12.7628	18.5625	14.2918
8	14.5508	21.9246	17.0775
10	16.2966	25.2924	20.1354
12	18.267	28.935	23.4924
14	19.948	32.8821	27.1697
16	22.2264	36.7035	30.4014
18	23.8431	40.206	34.5475
20	25.7344	45.7344	39.1339

8.3. Results for Nakagami-M Model

8.3.1. Simulation Curves showing the Results of Peak SNR vs Average SNR for the Nakagami-m Model using Three Different Modulation Techniques

The following simulation curves present the variation of PSNR with average SNR for the Nakagami-*m* fading channel model using three modulation schemes: BPSK without diversity, BPSK with 2-branch SC, and QPSK with 2-branch SC, evaluated on the ‘Bus’ and ‘People’ images. As the average SNR per branch increases from 0 to 20 dB, all three transmission schemes exhibit a consistent increase in PSNR, indicating progressive improvement in image reconstruction quality with better channel conditions. For e.g., in the simulation curve of the ‘Bus’ image, at 0 dB average SNR, the 2-SC BPSK scheme achieves PSNR of approximately 11.19 dB, while both no-diversity BPSK and 2-SC QPSK produce nearly 8.76 dB and 8.48 dB, respectively, providing an initial diversity gain of about 2.5 dB. At 10 dB average SNR, the PSNR values increase to approximately 28.24 dB for 2-SC BPSK, 21.99 dB for 2-SC QPSK, and 18.58 dB for no-diversity BPSK, representing improvements over the non-diversity system.

The advantage of diversity reception becomes more pronounced at higher SNR values. At 20 dB average SNR, 2-SC BPSK attains the highest PSNR of approximately 54 dB, followed by 2-SC QPSK at 46.40 dB, whereas no diversity BPSK reaches only 31.56 dB. Similarly, in the simulation curve of the ‘People’ image at 0 dB average SNR, the PSNR values are approximately 11.19 dB for 2-SC BPSK and 8.78 dB and 8.46 dB for both no-diversity BPSK and 2-SC QPSK, respectively, providing an initial diversity gain of about 2.5

dB. As the SNR increases to 10 dB, the PSNR improves to approximately 28.14 dB for 2-SC BPSK, 21.87 dB for 2-SC QPSK, and 18.41 dB for no diversity BPSK, representing improvements over the no diversity system. At higher SNR values, the performance advantage becomes more significant. At 20 dB average SNR, 2-SC BPSK attains the highest PSNR of approximately 54.18 dB, while 2-SC QPSK reaches about 43.77 dB and no diversity BPSK achieves only 31.30 dB. With PSNR values between 54.00 dB and 54.18 dB, the results unequivocally show that BPSK with 2-branch SC consistently provides the best performance for both images. This notable improvement demonstrates how SC diversity may effectively lessen the effects of fading, improving image reconstruction quality and guaranteeing more reliable wireless image transmission.

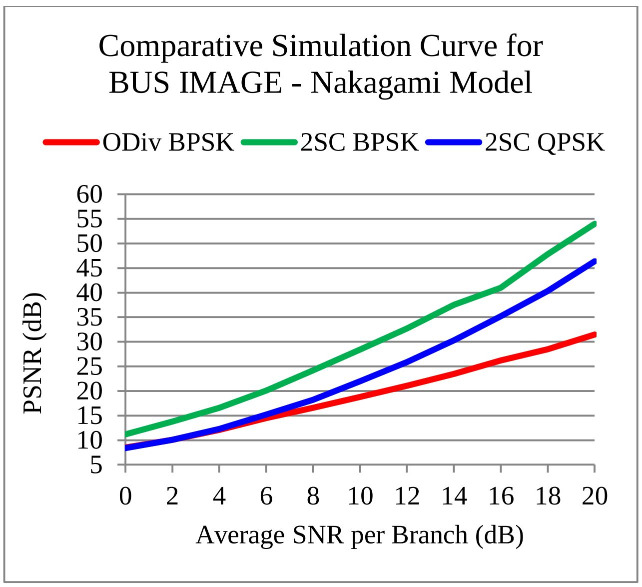

Fig. 6 Simulation curve showing the result for the bus image

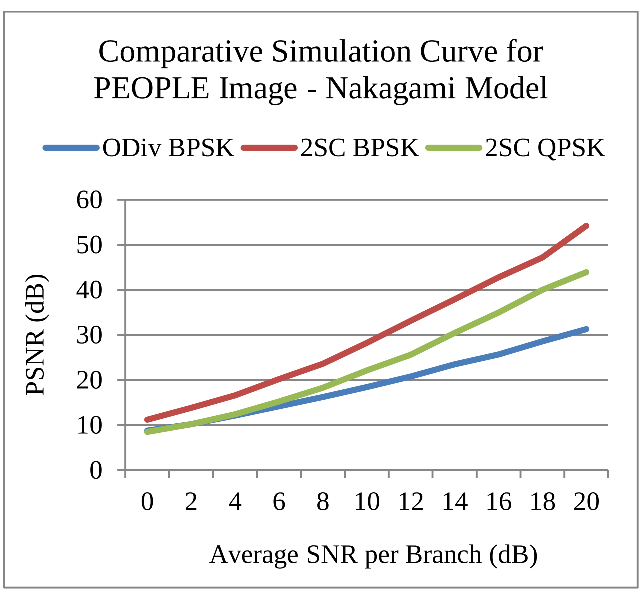

Fig. 7 Simulation curve showing the result for the people image

For the Nakagami-m fading channel, the PSNR values Vs Average SNR tables are prepared for both images and presented in Tables 4 and 5.

Table 4. Comparative Quality Analysis table showing the results of the Bus image

SNR (in dB)	PSNR (in dB) for modulation techniques		
	BPSK (0 DIV)	BPSK (2 SC)	QPSK (2 SC)
0	8.7655	11.1927	8.4884
2	10.2856	13.6739	10.1862
4	12.0737	16.6023	12.3057
6	14.1071	20.1817	15.0776
8	16.2966	24.057	18.0692
10	18.5863	28.2415	21.9922
12	20.9777	32.4828	26.0097
14	23.3504	37.5578	30.3472
16	26.0831	40.9632	35.3205
18	28.5269	47.9312	40.206
20	31.5609	54.0013	46.4039

Table 5. Comparative Quality Analysis table showing the results of the People image

SNR (in dB)	PSNR (in dB) for modulation techniques		
	BPSK (0 DIV)	BPSK (2 SC)	QPSK (2 SC)
0	8.7801	11.1903	8.4631
2	10.2418	13.6789	10.2041
4	12.0356	16.5384	12.3624
6	14.0574	20.1183	14.981
8	16.1549	23.6855	18.2393
10	18.4128	28.1431	21.8784
12	20.8671	33.0795	25.6484
14	23.624	37.8507	30.4014
16	25.7718	42.7241	34.9946
18	28.5863	47.1957	39.8718
20	31.3074	54.1854	43.7715

9. Conclusion

The experimental findings show that the suggested deep learning-based compression method effectively lowers image dimensionality while maintaining a high degree of visual fidelity. The autoencoder model outperforms conventional compression methods in terms of compression efficiency while preserving dependable reconstruction quality in a variety of scenarios. Promising findings were obtained from the performance evaluation.

To further explore its applicability in realistic wireless communication environments, the optimized compression framework was combined with channel models like the Rayleigh Fading Model and the Nakagami-m Fading Model under various modulation configurations with and without diversity techniques. The findings show that, even in situations with low SNR, the suggested approach retains superior visual quality and greatly increases the PSNR of reconstructed images. Specifically, diversity-assisted modulation techniques achieve PSNR values up to 55.18 dB, successfully mitigating channel impairments by lowering transmission errors and signal deterioration. Binary Phase Shift Keying with two-branch Selection was one of the assessed methods. Regarding visual quality and reconstruction accuracy, combining yields the best results. Overall, by lowering power and bandwidth needs while preserving high reconstruction accuracy, the suggested framework provides a dependable and effective wireless image transmission solution.

The steady gains in PSNR, MSE, SNR, and compression ratio attest to the resilience and efficiency of the suggested method in difficult wireless channel circumstances. For next-generation wireless multimedia communication systems that need dependable and effective image transmission, the suggested autoencoder-based compression technique thus offers a promising alternative. To further improve generative capabilities and representation learning across a larger range of wireless channel models, future research may investigate sophisticated architectures like Transformer Neural Networks.

References

[1] Shahzeb Hussain, Namrata Bhadri, and Md. Shaayan Hussain, “Advancements in Wireless Communication,” *International Journal of Electronics and Communication Engineering*, vol. 7, no. 9, pp. 1-4, 2020. [CrossRef] [Google Scholar] [Publisher Link]

[2] Mostafa Naseri et al., “Deep Learning-Based Image Compression for Wireless Communications: Impacts on Reliability, Throughput, and Latency,” *arXiv preprint*, pp. 1-13, 2024. [CrossRef] [Google Scholar] [Publisher Link]

[3] Chengsi Liang et al., “Generative AI-Driven Semantic Communication Networks: Architecture, Technologies and Applications,” *IEEE Transactions on Cognitive Communications and Networking*, vol. 11, no. 1, pp. 27-47, 2024. [CrossRef] [Google Scholar] [Publisher Link]

[4] Junhui Li, and Xingsong Hou, “Exploiting Inter-Image Similarity Prior for Low-Bitrate Remote Sensing Image Compression,” *arXiv preprint*, pp. 1-12, 2024. [CrossRef] [Google Scholar] [Publisher Link]

[5] Venkata Sankirtana Guntuboina, and Nishtha Srivastava, “Efficient Image Data Compression Techniques: A Comprehensive Review and Comparative Study,” *Research Square*, pp. 1-11, 2024. [CrossRef] [Google Scholar] [Publisher Link]

[6] Joshua Rajah Devadason, and Aju D, “A Comprehensive Survey of Image Compression Methods: From Prediction Models to Advanced Techniques,” *Multimedia Tools and Applications*, vol. 84, pp. 38653-38691, 2025. [CrossRef] [Google Scholar] [Publisher Link]

[7] Murooj Khalid Ibraheem Ibraheem, Alexander Viktorovich Dvorkovich, and Israa M. Abdalameer Al-khafaji, “A Comprehensive Literature Review on Image and Video Compression: Trends, Algorithms, and Techniques,” *Information Systems Engineering*, vol. 29, no. 3, pp. 863-876, 2024. [CrossRef] [Google Scholar] [Publisher Link]

[8] G.K. Wallace, “The JPEG Still Picture Compression Standard,” *IEEE Transactions on Consumer Electronics*, vol. 387, no. 1, pp. 18-34, 1992. [CrossRef] [Google Scholar] [Publisher Link]

[9] Akane Shoda, Tomo Miyazaki, and Shinichiro Omachi “JPEG Image Enhancement with Pre-Processing of Color Reduction and Smoothing,” *Sensors*, vol. 23, no. 21, pp.1-16, 2023. [CrossRef] [Google Scholar] [Publisher Link]

[10] C. Christopoulos, A. Skodras, and T. Ebrahimi, “The JPEG2000 Still Image Coding System: An Overview,” *IEEE Transactions on Consumer Electronics*, vol. 46, no. 4, pp. 1103-1127, 2000. [CrossRef] [Google Scholar] [Publisher Link]

[11] M.W. Marcellin et al., “An Overview of JPEG-2000,” *Proceedings DCC 2000. Data Compression Conference, Snowbird*, UT, USA, pp. 523-541, 2000. [CrossRef] [Google Scholar] [Publisher Link]

[12] Miao Zhang et al., “Joint Lossless Image Compression and Encryption Scheme based on CALIC and Hyperchaotic System,” *Entropy*, vol. 23, no. 8, pp. 1-29, 2021. [CrossRef] [Google Scholar] [Publisher Link]

[13] Nuzhat Mobeen, Channappa A, and Suresh B, “Image Compression Methods for Efficient Storage and Transmission,” *World Journal of Advanced Research and Reviews*, vol. 11, no. 1, pp. 265-278, 2021. [CrossRef] [Google Scholar] [Publisher Link]

[14] Manish I. Patel, Sirali Suthar, and Jil Thakar, “Survey on Image Compression using Machine Learning and Deep Learning,” *2019 International Conference on Intelligent Computing and Control Systems (ICCS)*, Madurai, India, pp. 1103-1105, 2019. [CrossRef] [Google Scholar] [Publisher Link]

[15] Irina Marcheko et al., “Image Compression Research Based On Convolutional Autoencoder,” *Information Control Systems and Technologies (IUST-ODESA-2025): Proceedings of the 13th International Scientific and Practical Conference*, Odessa, pp. 24-26, 2025. [Google Scholar] [Publisher Link]

[16] Lucas Theis et al., "Lossy Image Compression with Compressive Autoencoders," *arXiv preprint*, pp. 1-19, 2017. [CrossRef] [Google Scholar] [Publisher Link]

[17] Yixin Mei et al., "Learning-Based Scalable Image Compression with Latent-Feature Reuse and Prediction," *IEEE Transactions on Multimedia*, vol. 24, pp. 4143-4157, 2021. [CrossRef] [Google Scholar] [Publisher Link]

[18] Zhengxue Cheng et al., "Deep Convolutional Autoencoder-based Lossy Image Compression," *2018 Picture Coding Symposium (PCS)*, San Francisco, CA, USA, pp. 253-257, 2018. [CrossRef] [Google Scholar] [Publisher Link]

[19] M. Aiswarya, Jwala Jose, and S. Sritha, "A Review on Image Compression Techniques," *International Journal of Innovative Research in Technology*, vol. 11, no. 7, pp. 1-5, 2024. [Google Scholar] [Publisher Link]

[20] Renuka Girish Deshpande, Lata L. Ragha, and Satyendra Kumar Sharma, "Video Quality Assessment through PSNR Estimation for Different Compression Standards," *Indonesian Journal of Electrical Engineering and Computer Science*, vol. 11, no. 3, pp. 918-924, 2018. [CrossRef] [Google Scholar] [Publisher Link]

[21] Umme Sara, Morium Akter, and Mohammad Shorif Uddin, "Image Quality Assessment through FSIM, SSIM, MSE, and PSNR—A Comparative Study," *Journal of Computer and Communications*, vol. 7, no. 3, pp. 8-18, 2019. [CrossRef] [Google Scholar] [Publisher Link]

[22] Vlad-Ilie Ungureanu, Paul Negirla, and Adrian Korodi, "Image-Compression Techniques: Classical and "Region-of-Interest-Based" Approaches Presented in Recent Papers," *Sensors*, vol. 24, no. 3, pp. 1-27, 2024. [CrossRef] [Google Scholar] [Publisher Link]

[23] COCO Dataset 2017, Kaggle. [Online]. Available: https://www.kaggle.com/datasets/sabahesaraki/2017-2017

[24] Swasti Jain et al., "Object Detection using the COCO Dataset," *2022 International Conference on Cyber Resilience (ICCR)*, Dubai, United Arab Emirates, pp. 1-4, 2022. [CrossRef] [Google Scholar] [Publisher Link]

[25] Faris Keti, "Diversity Techniques in Wireless Communication Systems: A Review," *European Journal of Theoretical and Applied Sciences*, vol. 1, no. 6, pp. 431-440, 2023. [CrossRef] [Google Scholar] [Publisher Link]

[26] Satyanand Choudhary, Surbhi Jha, and Prabhakar Sharma, "A Review of Diversity Techniques in Wireless Communication System," *Proceedings of National Conference on Recent Advances in Electronics and Communication Engineering*, pp. 1-6, 2014. [Google Scholar] [Publisher Link]

[27] Raghunath Mandal et al., "Performance Evaluation of Selection Combiner Under Different Wireless Mobile Fading Channels-A Review," *2024 2nd International Conference on Device Intelligence, Computing and Communication Technologies (DICCT)*, Dehradun, India, pp. 163-168, 2024. [CrossRef] [Google Scholar] [Publisher Link]

[28] Osamah S. Badarneh et al., "Selection Combining Over the Extended Fading Channels," *IEEE Wireless Communications Letters*, vol. 11, no. 4, pp. 722-726, 2022. [CrossRef] [Google Scholar] [Publisher Link]

[29] Jai Kumar et al., "A Review on 5G and Beyond Wireless Communication Channel Models: Applications and Challenges," *Physical Communication*, vol. 67, 2024. [CrossRef] [Google Scholar] [Publisher Link]

[30] T.S. Rappaport, *Wireless Communications: Principles and Practice, 2/E*, Pearson Education India, pp. 1-736, 2010. [Google Scholar] [Publisher Link]

[31] V.A. Aalo, "Performance of Maximal-Ratio Diversity Systems in a Correlated Nakagami-Fading Environment," *IEEE Transactions on Communications*, vol. 43, no. 8, pp. 2360-2369, 2002. [CrossRef] [Google Scholar] [Publisher Link]

[32] Emil Björnson, and Luca Sanguinetti, "Rayleigh Fading Modelling and Channel Hardening for Reconfigurable Intelligent Surfaces," *IEEE Wireless Communications Letters*, vol. 10, no. 4, pp. 830-834, 2020. [CrossRef] [Google Scholar] [Publisher Link]

[33] Marvin K. Simon, and Mohamed-Slim Alouini, *Digital Communication over Fading Channels*, John Wiley & Sons, 2004. [CrossRef] [Google Scholar] [Publisher Link]

[34] Neelam Srivastava, Arpita Johri, and Mudit Saxena, "Performance of Nakagami–m Fading Channel with Equal Gain Combining and Maximal Ratio Combining Diversity Techniques," *International Journal of Electronics Communication and Computer Engineering*, vol. 3, no. 1, pp. 46-52, 2012. [Google Scholar] [Publisher Link]

[35] I. S. Gradshteyn, and I. M. Ryzhik, *Table of Integrals, Series, and Products*, Academic Press, pp. 1-1206, 2014. [Google Scholar] [Publisher Link]

[36] Samar Kumar Rony, Farhana Akter Mou, and Md. Moshiur Rahman, "Performance Analysis of OFDM Signal using BPSK and QPSK Modulation Techniques," *American Journal of Engineering Research*, vol. 6, no. 1, pp. 108-117, 2017. [Google Scholar] [Publisher Link]

[37] R. Devi, and H. Nishat, "Performance Evaluation of Digital Modulation Schemes BPSK, QPSK, QAM," *International Journal Engineering Technology*, vol. 3, no. 2, pp. 71-74, 2017. [Google Scholar]